energy&fuels

pubs.acs.org/EF

Article

Enhanced Oil Recovery through Microbially Induced Calcium Carbonate Precipitation

Shunxiang Xia, Artur Davletshin, and Wen Song*

Cite This: *Energy Fuels* 2023, 37, 14666−14673

Read Online

ACCESS | Metrics & More | Article Recommendations

ABSTRACT: Mobility contrasts between oil and water, along with permeability heterogeneity, lead to fingering instabilities that impede the recovery of hydrocarbons from the subsurface. Here, we present a novel, improved oil recovery approach, whereby microbially induced carbonate precipitation (MICP) reduces the local permeability of water-saturated preferential flow paths to improve the overall sweep of the reservoir. With MICP, local pore geometry in preferential pathways is altered to divert successive injection fluids to oil-saturated pores. We demonstrate the feasibility of the approach using a silicon microfluidic device with etched geometries representative of real rock pores, where a ∼5% reduction in the local porosity of water-swept regions increased overall oil recovery by ∼28% original oil in place (OOIP). We performed sensitivity analysis on the injection conditions required to maximize oil recovery and bacterial growth. Overall, we show that calcium carbonate grains grown using MICP can provide a secure and stable method to control fluid flow *in situ* and recover additional hydrocarbons to provide an avenue for cost-effective and environmentally benign hydrocarbon extraction.

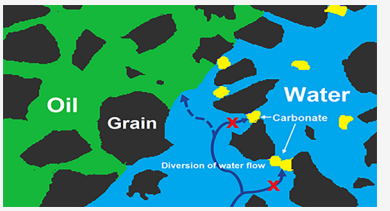

1. INTRODUCTION

Crude oil resources supplied more than 50% of the world's energy needs in 2021, with demand projected to increase for the foreseeable future.[1] To ensure energy security and to alleviate negative impacts of hydrocarbon extraction on the environment, methods to improve oil recovery in environmentally benign (i.e., nontoxic and chemically stable) manners are needed.[2] Current waterflooding approaches (i.e., injection of brine into the reservoir) are limited to ∼35% recovery of the original oil in place (OOIP) as a result of complex multiphase fluids transport through heterogeneous geomaterials[3] and leave much of the available hydrocarbons inaccessible.

One approach to improving overall hydrocarbon recovery lies in increasing the sweep efficiency of the reservoir (i.e., the volume of the reservoir contacted by the injected fluid). For example, cross-linking injected materials such as silica gels, polyacrylamide and hydrolyzed polyacrylamide, xanthan gum, and guar gum within preferential flow paths reduces the local permeability and diverts subsequent injection fluids away into oil-saturated pores.[4] Despite extensive efforts, cross-linked polymeric cements have proven unstable in harsh geologic environments with elevated temperature, pH, salinity, multivalent ions, and high shear rates during injection.[5]

Here, we present an *in situ* biogenic approach that alters the morphology of preferential flow paths and redirects injection fluids to recover oil from previously unswept pores. We leverage naturally occurring carbonate-secreting microbes found in groundwater systems that promote calcium carbonate precipitation (i.e., microbially induced carbonate precipitation, or MICP).[6−8] Specifically, *Sporosarcina pasteurii*, a urease bacteria, is of interest here because of their low culture cost, ease of culturing, strong adaptability to harsh environments, and resistance to aggregation.[9] Here, the overall reactions involved in biogenic calcium carbonate precipitation are[10]

$$CO(NH_2)_2 + 2H_2O \rightarrow 2NH_4^+ + CO_3^{2-} \quad (1)$$

$$CO_3^{2-} + Ca^{2+} \rightarrow CaCO_3 \quad (2)$$

During MICP, the bacteria secrete urease to catalyze the decomposition of urea into carbonate (CO_3^{2-}) and ammonia (NH_4^+) ions (eq 1). Simultaneously, the negatively charged surface of the bacteria adsorb Ca^{2+} from the brine, that once in contact with carbonate ions, precipitates calcium carbonate ($CaCO_{3(s)}$).[11] Calcium carbonate precipitation occurs most frequently in proximity to the microbial colony and hence reduces the local permeability of bacteria-abundant soils.[9]

To induce MICP in the subsurface, microbial introduction and culturing mimicking natural growth processes in the targeted medium are required. In previous MICP groundwater remediation efforts, a microbial suspension is injected into the soil, followed by nutrient delivery to promote *in situ* bacteria growth and urease secretion. Following sufficient microbial growth, MICP is induced by injecting a cementation solution

Received: June 7, 2023
Revised: August 31, 2023
Published: September 20, 2023

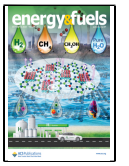

of urea and calcium to reduce the local porosity and permeability of the reservoir.

While both lab- and field-scale studies show that MICP is affected strongly by injection conditions (e.g., flow rates, concentrations, etc.), understanding of the controls on the spatiotemporal changes to flow patterns and sweep efficiency is lacking.[12,13] The injection and transport of bacteria into the formation are crucial to the success of MICP. Cui et al. investigated the transport behavior of *S. pasteurii* in sandstone and found that the bacteria tend to aggregate and clog at pore throats at low superficial velocities, limiting the spatial distribution of microbes and resulting in poor cementation.[14] With the help of X-ray computed tomography (CT), Minto et al. observed heterogeneities in the reduction of porosity and permeability within the core sample as a result of poor bacteria transport through the porous medium.[15] In addition to bacteria deposition into rock, the success of an MICP-based enhancing oil recovery (EOR) approach depends also on the ability to precipitate calcium carbonate within the porous medium. Specifically, the rate of MICP and the spatial distribution of calcium carbonate precipitates are influenced strongly by geologic and injection conditions, including reservoir temperature and pH, bacteria density, injection rate, and injection fluid composition.[15] Wang et al. studied the effects of bacterial density on the growth kinetics of calcium carbonates and pointed out that MICP is rate-limited by urea degradation.[16] Achal and Pan investigated the performance of MICP with different calcium carbonate sources and found that calcium chloride provided the highest urease activity and calcium carbonate yield.[17] The strength of the cementation is determined by the mass and local distribution of calcium carbonates within the pore space. Sham et al. applied magnetic resonance imaging (MRI) during MICP to reveal the spatial variation in calcium carbonate inside a Bentheimer sandstone core and studied its effect on the cementation strength.[18] Interestingly, bacteria provide a preferential nucleation site for calcium carbonate precipitation.[19] Bulk and core flooding experiments by Larsen et al. and Miao et al. showed that MCIP enhances oil recovery by reducing the porosity of the reservoir,[20,21] although mechanistic understanding of the interactions between the bacteria, reservoir fluids, and mineral grains remains unresolved. To elucidate the fundamental processes governing MICP in porous media, spatiotemporal resolution of the pore-scale processes is required.

Microfluidic platforms, paired with optical microscopy, offer an opportunity to study the fundamental pore-level interactions between microbes and reservoir fluids in confined rock environments to understand and control MICP-enabled hydrocarbon recovery. While microfluidics have been used previously to investigate the impact of MICP on pore morphology, these studies rely on the use of artificial porous media comprised of simple channel geometries (i.e., linear or cylindrical flow geometries) fabricated using polymeric materials [e.g., poly(dimethylsiloxane), PDMS] that fail to replicate the representative pore geometry and surface chemistry of geologic formations.[30−32] Recent developments in geochemical microfluidics enable the direct visualization of pore-scale (∼μm) phenomena in real time (∼ms) to resolve complex multiphase transport dynamics within geomaterials.[22−29] For example, Song et al. introduced calcite-based and carbonate-functionalized micromodels to investigate the reactive transport mechanisms underlying carbonate dissolution to assess the security of geologic carbon sequestration.[23,24]

In this study, we investigate the influence of MICP in enhanced oil recovery (EOR) using a micromodel with representative pore geometry of a sandstone to elucidate microbial delivery and local pore morphology alteration during MICP. Bacteria and cementation solutions were injected into the micromodel to induce MICP, and the cementation effect was studied at the pore scale via direct visualization. Notably, hydrocarbon recovery was improved by ∼28% OOIP following MICP-induced flow diversion.

2. MATERIALS AND METHODS

2.1. Micromodel Fabrication. Pore-scale visualization of MICP-based EOR was achieved using a microfluidic platform with a geometry representative of geologic media (i.e., micromodel). Specifically, an etched-silicon micromodel (30 mm by 20 mm) was fabricated using standard photolithography techniques following previous work.[25] In short, a silicon wafer (University Wafer Inc.) was etched with a depth of 10 μm by using the Bosch process (Plasma Lab 80+, Oxford Instruments) to achieve the representative pore geometry of sandstone and to allow for pore-scale flow visualization. Next, the etched silicon wafer was bonded anodically to Schott Borofloat 33 glass (University Wafer Inc.) to visualize the reactive transport dynamics during MICP.

2.2. Bacteria Culture and Viability in Water−Oil Mixture. The bacterium *S. pasteurii* (ATCC 11859) was chosen due to its well-documented ability to grow on solid surfaces and its capacity to precipitate calcium carbonate minerals under both aerobic and anaerobic conditions.[33] The bacteria were cultivated in a growth medium before injection into the micromodels. The growth medium was prepared by dissolving 20 g of yeast extract (CAS-NO: 8013012, MilliporeSigma) and 10 g of ammonium sulfate (CAS-NO: 7783202, Sigma-Aldrich) into 1 L of deionized (DI) that was then sterilized for 15 min at 121 °C in an autoclave. Bacteria were inoculated into the growth medium and incubated at room temperature for 3 days to encourage growth.

To assess the viability of *S. pasteurii* growth and urease stability toward improved oil recovery, we quantified bacterial growth dynamics in proximity to crude oil. Specifically, 3 mL of crude oil (Table 1) was added to a bacteria broth (1 vol % bacterial inoculated with 30 mL of growth medium) in a glass bottle. The oil/microbe medium was rotated at 100 rpm to prevent microbial settling. The cell density of the solution, indicated by the optical density at 660 nm (OD_{660}), was measured every 12 h using a spectrum photometer (Cary 60 UV−vis, Agilent) to quantify microbial growth rates. The urease activity of bacterial broth was determined by the Berthlot method, where one unit of urease activity was defined as 1 mM of ammonia produced per minute at room temperature.[34]

Table 1. Properties of Crude Oil

crude oil properties	value
acid number (mg/g)	2.36
base number (mg/g)	6.02
asphaltene content (wt %)	2.69
density (°API)	21
viscosity at 22.8 °C (cP)	105.7

2.3. Pore-Scale Visualization. Reservoir fluid displacement, bacteria transport, and calcium carbonate growth within the microfluidic system were visualized using a microscope (Nikon Eclipse Lvdia-N) and camera (Nikon Ds-fi3) (Figure 1). A micromodel (30 mm by 20 mm) with pore geometry representative of a sandstone (porosity ∼54%, permeability 800 mD,[25] etch depth ∼10 μm) was used to visualize improvements to oil recovery via MICP. The average size of pore bodies and throats of the microfluidic network were 58 and 13 μm, respectively. Fluid displacement and calcium carbonate growth were monitored under bright-field and polarized light microscopy, respectively. Microbial attachment along

https://doi.org/10.1021/acs.energyfuels.3c02027
Energy Fuels 2023, 37, 14666−14673

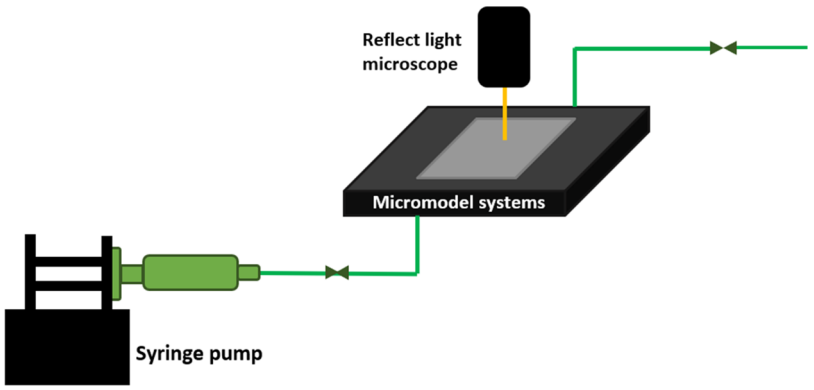

Figure 1. Schematic of the microvisualization platform.

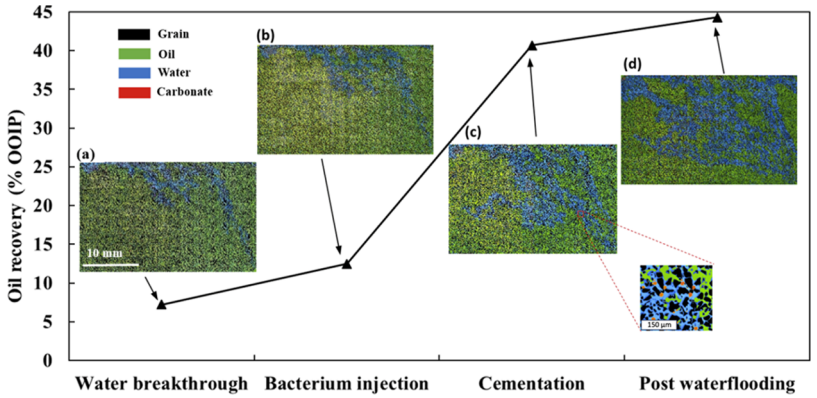

Figure 2. Oil recovery during the four stages of MICP-EOR using large images (i.e., 21 × 13 micrographs stitched) of the micromodel. In the micrographs, the grains, oil, water, and carbonate are denoted by black, green, blue, and red, respectively. (a) Water breakthrough following an initial waterflood with 20,000 ppm brine recovered ∼7% of the OOIP. (b) Injection of *S. pasteurii* caused a slight increase in water saturation because of microbial accumulation and blockage at pore throats. (c) Injection of cementation solution containing 1 M $CaCl_2$ and 1 M urea at 0.08 m per day for 40 h was performed to initiate *in situ* MICP. Injected fluids were redirected through oil-saturated pores and increased the oil recovery by an additional ∼28% OOIP. (d) Post-MICP waterflooding recovered an additional ∼5% OOIP.

porous micromodel surfaces was imaged using dark-field microscopy. Brine (20,000 ppm of NaCl) and crude oil were injected into the micromodel using a syringe pump (Harvard Apparatus) at a typical superficial velocity of 0.8 m/day to establish initial reservoir conditions.[35] Brine was then injected into micromodel at 0.8 m/day to mimic a waterflood, where water breakthrough via the formation of a preferential water path was achieved after ∼0.1 pore volumes (PV, ∼5 min) of injection. Finally, one PV of 3-day incubated bacteria broth was injected into the micromodel for 20 min, after which the system was kept static for 2 h to encourage microbial attachment on pore surfaces.

MICP-EOR was enabled by injecting a cementation solution containing Ca^{2+} and urea into the micromodel. The influence of Ca^{2+} concentration and injection velocity on the rate and spatial distribution of calcium carbonate precipitates was assessed by injecting solutions with concentrations of 1, 0.5, and 0.25 M Ca^{2+} continuously at superficial velocities of 0.08, 0.16, and 0.32 m/day. For alternating injection/shut-in conditions, on the other hand, the impact of microbial growth and solution residence time on carbonate precipitation was assessed by alternating between constant flow and no flow conditions such that the cementation solution was injected continuously for 5 h, followed by 5 h of quiescence. Large (whole micromodels) micrographs were captured after 4 and 8 pore volumes (PV) of cementation to visualize the pore- and pore-ensemble growths of calcium carbonate within the porous medium. Here, we assume that fluid distributions in the depth of view are constant (i.e., the micromodel is a two-dimensional (2D) device) because of the thin etch depth (∼10 μm). As a result, all calculated quantities are derived from area measurements, assuming uniformity in the depth direction. All quantification, including oil recovery, was calculated by image segmentation using a convolution neural network (CNN)-based image processing algorithm.[36] We measure oil recoveries across the micromodel and report a single averaged quantity taken from 273 (21 by 13) fields of view. In each field of view, the oil recovery was calculated as the ratio of the area occupied by oil to the initial area occupied by oil (i.e., $A_o(t)/A_o(t_0)$). A control experiment was conducted by injecting 8 PV of a cementation solution containing 1 M $CaCl_2$ and 1 M urea at 0.08 m/day after the water breakthrough without bacteria. Here, no microbes were present to delineate the impact of MICP on improving hydrocarbon recovery.

3. RESULTS AND DISCUSSION

3.1. Enhanced Oil Recovery with Flow Diversion. Using MICP, overall oil recovery increased by ∼28% of the original oil in place (OOIP, Figure 2). Importantly, direct visualization of the geochemical micromodel showed significant flow diversion from the initial preferential flow paths following carbonate precipitation.

Prior to MICP-EOR, waterflooding resulted in the development of a narrow preferential flow path (Figure 2a) that limited overall oil recovery to ∼7% OOIP. Microbial injection and deposition in the preferential flow paths (Figure 2b) resulted in minor changes in overall increase in oil recovery (∼5% OOIP, Figure 2b). MICP notably reduced the local porosity and pore connectivity of the water-swept flow paths and diverted subsequent fluids into oil-bearing pores that were

https://doi.org/10.1021/acs.energyfuels.3c02027
Energy Fuels 2023, 37, 14666−14673

previously unswept (Figure 2c). As a result, MICP here improved the overall oil recovery by an additional ~28% OOIP (Figure 2c). Subsequent waterflooding increased oil recovery by ~5% OOIP (Figure 2d). We note that in the control experiment where no microbes were present (i.e., no MICP), overall oil recovery increased by only ~5.5% OOIP, suggesting that the mass transfer between cementation fluids and the oil phase has a limited effect on improving oil recovery.

A control on the increase in sweep efficiency of MICP-EOR is the spatial distribution of calcium carbonate grains precipitated. Here, we leverage the proximity of MICP to bacterial colonies. Specifically, bacteria were deposited preferentially in the water-saturated flow paths because of the low local resistance to flow (i.e., higher local saturation and relative permeability). Similarly, the transport of cementation fluids favored the water-saturated channels ($S_w \sim 1$) and resulted in carbonate precipitation within the high water-saturation flow paths. As a result of the local reduction in porosity, permeability was decreased within the water-saturated zones, and subsequent fluids were diverted elsewhere (i.e., oil-saturated regions of the porous medium).

During cementation, calcium carbonate crystals precipitated primarily in the water phase. Here, we discretize the micromodel to representative elementary volumes (REVs, ~300 μm × 300 μm × 10 μm, ~10−15 pore bodies) and quantified local calcium carbonate volumes in each REVs (Figure 3). Notably, carbonate precipitation occurred only in the water-swept regions, where microbes were present. Measurements enabled by image processing show a positive correlation between local carbonate mineral content and water saturation (S_w, ratio of the volume of water to the total volume of fluid) (Figure 3a). In water-swept REVs ($S_w \geq 20\%$), local porosity was reduced by 5% (between 0 and up to ~47%,

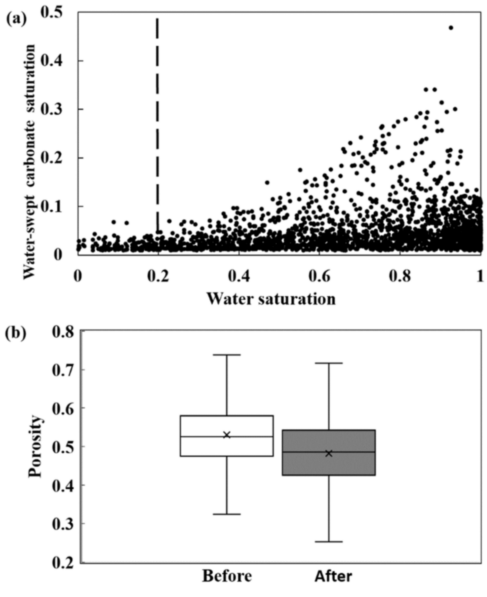

Figure 3. Characterization of calcium carbonate growth within the multiphase porous system. (a) Carbonate saturation (i.e., the ratio of the volume of calcium carbonate to the initial pore volume) in the water-swept regions increases with water saturation (i.e., water volume normalized by total fluid volume) over the 2143 REVs sampled across the micromodel (each REV comprises a 300 × 300 μm field of view). (b) Porosity of the water-swept REVs decreased from ~54 to ~48% as a result of MICP.

Figure 3b). A minimum water saturation required to enable MICP was found to be $S_w \sim 20\%$. Some carbonate precipitates were found in low water-saturation REVs (i.e., oil-filled REVs, $S_w < 0.2$), where mobilized oil had been redeposited. In general, MICP occurred in water-saturated REVs to which bacteria and Ca^{2+} could be delivered.

3.2. Pore-Scale Calcium Carbonate Growth. To understand and control the overall performance of MICP in porous media, we imaged the pore-scale precipitation of carbonate minerals within the micromodel in real time (~ms, Figure 4). After 2 h of cementation, carbonate crystals were

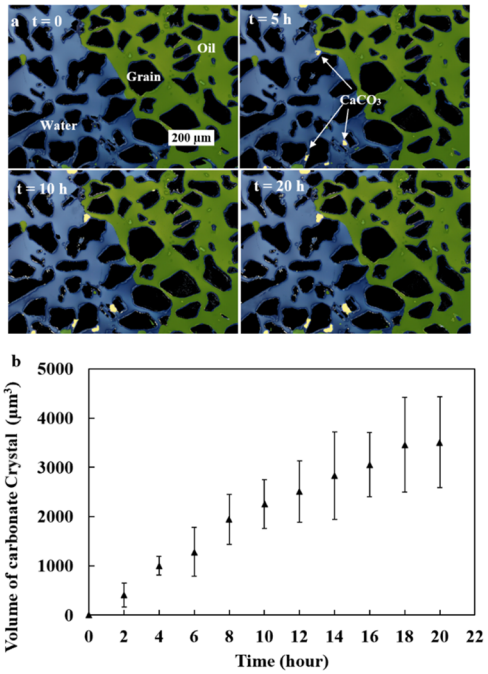

Figure 4. (a) Growth of calcium carbonate in the micromodel as a result of cementation solution injected at 0.15 m/day. The grain, oil, and water are denoted by black, green, and blue, respectively. Calcium carbonate is highlighted in yellow. (b) Average volume of carbonate grains increases approximately linearly with time and suggests that the process is limited by the transport of carbonate ions that were produced by the bacterial urease to the reaction interface. Error bars show the variation in growth rates from 5 precipitates.

observed at pore throats where the attached microbes provided nucleation sites (Figure 4a). Interestingly, once the small crystals precipitated, subsequent cementation resulted in only the growth of the existing crystals instead of additional nucleation on the microbes (Figure 4a).

During cementation (i.e., injection of 1 M $CaCl_2$ and 1 M urea at a superficial velocity of 0.08 m/day), individual carbonate grains grew at a rate of ~174 μm^3/h (Figure 4b). Despite the increase in carbonate surface areas available for precipitation, the constant rate of MICP suggests that the overall precipitation reaction was limited by the production and transport of carbonate ions enabled by bacterial urease to the reaction surface.

3.3. Bacteria Attachment and Viability in the Porous Medium. In this study, the rod-like bacteria were immobilized in the micromodel primarily via surface attachment (Figure 5a) rather than pore-clogging (Figure 5b). Specifically, *S. pasteurii* secrete extracellular polymeric substances (EPS) to enable attachment on silicate pore surfaces.[11] Microbial immobiliza-

https://doi.org/10.1021/acs.energyfuels.3c02027
Energy Fuels 2023, 37, 14666−14673

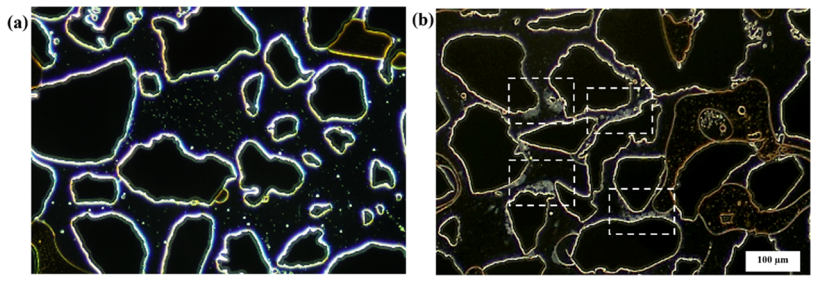

Figure 5. Dark-field micrographs of bacteria (a) attached to pore surfaces and (b) clogged in pore throats.

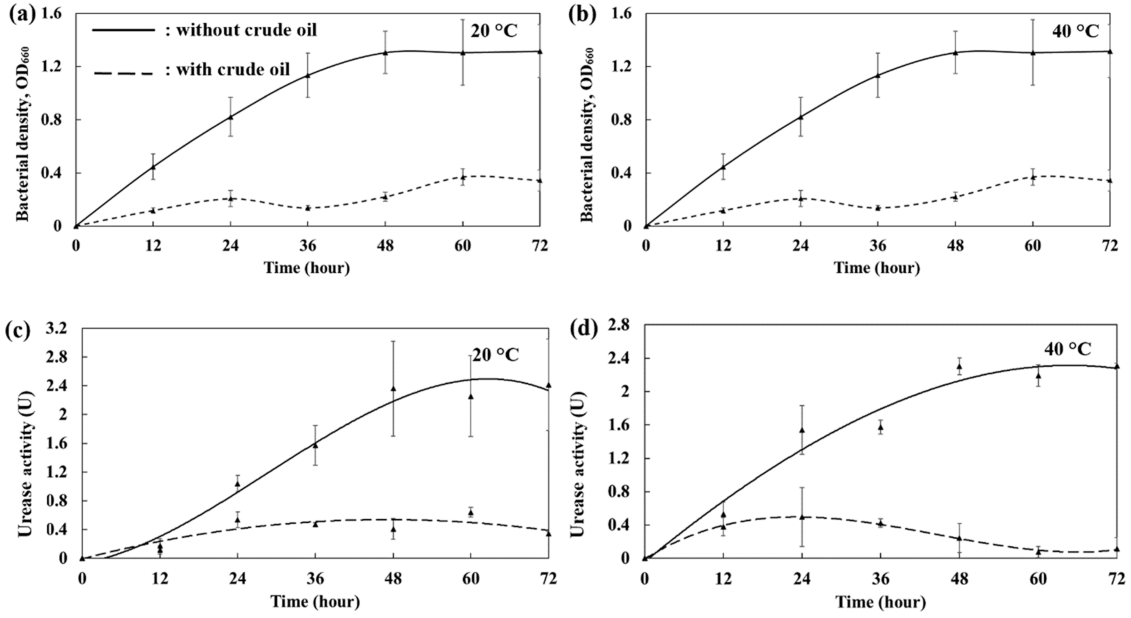

Figure 6. Growth curve and urease activity of *S. pasteurii* during culture at 20 °C (a, c) and 40 °C (b, d). Dashed and solid lines represent the cultures of *S. pasteurii* with and without crude oil, respectively. One unit of urease activity was defined as 1 mM of ammonia produced per minute at room temperature.

tion in small pore throats was also observed, albeit less frequently, where the rod-like bacterial clog the narrow flow paths (Figure 5b).[37]

Once attached to the pore surface, the feasibility of using bacteria to induce calcium carbonate precipitation *in situ* relies on their viability under extreme geologic conditions (i.e., elevated temperatures, pressures, salinities, presence of crude oils, etc.).[38] Specifically, the influence of elevated temperature on microbial growth and enzyme activity must be understood.[39] In this work, the impact of temperature on bacterial growth was observed only for temperatures above 50 °C. For temperatures below 50 °C, both the microbial cell density and enzyme activity increased continuously over time until the maximum values (1.25 OD and 2.35 U) were reached after 2 days of culturing (Figure 6, solid lines). Elevated temperatures (40 °C, Figure 6b,d) increased the growth rate of the bacteria at early times (i.e., during the first day), but the maximum value of cell density and enzyme activity remained constant.

The influence of crude oil on the growth and productivity of *S. pasteurii* was assessed by measuring the microbial cell density and enzyme activity upon exposure to crude oil. In comparison to those measured in the absence of crude oil, the maximum cell density and enzyme activity of microbes in the proximity of crude oil decreased by ∼73.1 and 71.6%, respectively (i.e.,. 34 OD and 0.66 U; Figure 6a,c, dashed lines). The inhibition of crude oil on cell growth and productivity was exacerbated for elevated temperatures (e.g., at 40 °C). Diffusive partitioning of toxic crude oil components into the water phase is enhanced at elevated temperatures, thereby interfering with the microbial colony productivity (Figure 6b,d, dashed lines).[40] Favorably, the inhibitive effect of crude oils on bacteria growth offers a unique opportunity for selective carbonate precipitation within the water-saturated zones (e.g., viscous fingers) as opposed to traditional approaches that are aspecific to the fluid saturations within the reservoir.[41] Here, the bacteria grow preferentially in regions of the reservoir with high water saturation (i.e., low oil saturation) and precipitate calcium carbonate grains locally. The result, importantly, is that the pore-connectivity within the initially water-swept regions is reduced, and successive fluids are diverted to oil-saturated (i.e., unswept) regions of the reservoir to improve overall recovery.[42,43] We note here that the EPS secreted by *S. pasteurii* tends to increase the oil wettability of the local environment and is expected to limit improvements to oil recovery, in contrast to our observations. As a result, we deduce that the main mechanism leading to improved oil recovery here is flow diversion via carbonate precipitation and increased sweep efficiency of the reservoir.

3.4. Sensitivity Analysis of the Injection Conditions.

The influence of injection conditions (i.e., injection rate, concentration of cementation fluid, injection patterns) on

https://doi.org/10.1021/acs.energyfuels.3c02027
Energy Fuels 2023, 37, 14666−14673

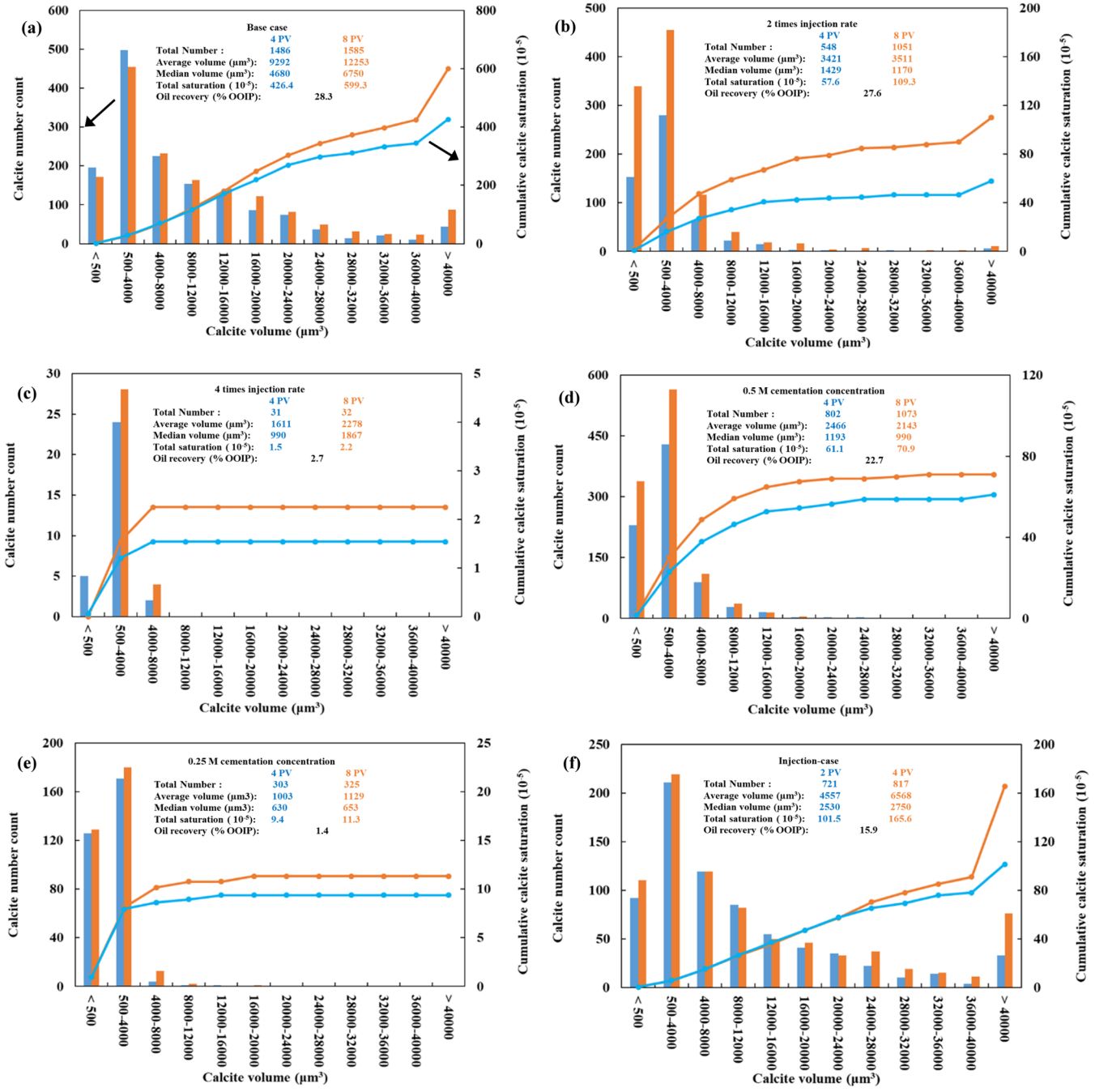

Figure 7. Size distribution and saturation of precipitated calcium carbonate grains after various conditions of cementation. The blue and orange columns represent the occurrence frequency of calcium carbonate grain sizes at 50 and 100% of the cementation period, respectively. The blue and orange lines represent cumulative calcium carbonate saturation at 50 and 100% of the cementation period, respectively. For the base case (a), a cementation solution of 1 M $CaCl_2$ and 1 M urea was injected at a superficial velocity of ~0.08 m/day. Increased injection velocities at 0.16 (b) and 0.32 m/day (c) show that for short residence times associated with high injection velocities, urea cannot be degraded by the bacteria in time to provide the necessary bicarbonate ions for calcium carbonate precipitation. Diluting the concentration of $CaCl_2$ and urea to 0.5 M (d) and 0.25 M (e) shows that decreasing the solution concentration shifts the reaction equilibrium and leads to decreases in calcium carbonate precipitate. Alternating between constant and no flow injections (f) also resulted in less carbonate precipitation due to the loss of bacteria enzyme activity during the process. The oil recovery was calculated by using changes to oil saturation due to cementation.

MICP-EOR was assessed to optimize hydrocarbon recovery (Figure 7). Data for the full set of experiments are taken from single experimental runs; however, multiplicates were performed that show similar trends. We set the base case scenario by injecting a cementation solution of 1 M $CaCl_2$ and urea at a superficial velocity of 0.08 m/day. In all cases, the median carbonate grain size shifted toward larger crystals at later times (e.g., ~4680 μm^3 after 4 PV and 6750 μm^3 after 8 PV of cementation fluid injection for the base case, Figure 7a). Recall that for a fixed solution concentration and injection rate, additional injection results in the enlargement of individual carbonate mineral grains, as opposed to the nucleation of new crystals. This coarsening in the carbonate grain size distribution is caused by the preferential growth of $CaCO_3$

https://doi.org/10.1021/acs.energyfuels.3c02027
Energy Fuels 2023, 37, 14666−14673

on existing mineral surfaces. Across the micromodel "reservoir" (2 × 3 cm), the overall porosity of the whole micromodel (including unswept regions) decreased by ∼0.6% after 8 PV of precipitation. While this is a small change in the total porosity of the reservoir, we note that the change in porosity is localized to water-swept flow paths, where local porosity decreased by ∼5% and resulted in significant flow diversion. Overall, carbonate precipitation in the water-saturated flow paths leads to an improved oil recovery of ∼28% OOIP.

We probe the influence of injection rate on porosity alteration by examining carbonate mineral growth at 2 and 4 times the velocity of the base case scenario (i.e., superficial velocities of 0.16 and 0.32 m/day, Figure 7b,c). Here, we find that carbonate precipitation is delayed with increasing injection velocity (i.e., precipitation is distributed further downstream). Specifically, overall carbonate precipitation (i.e., calcium carbonate number and size) decreased with higher injection rates. Doubling the injection rate resulted in a 6-fold decrease in carbonate precipitation and decreased the median volume of carbonate grains from 6750 to 1170 μm^3. At 0.32 m/day, MICP was inhibited, and only 32 calcium carbonate crystals were observed across the micromodel, suggesting that the transport of carbonate ions was limited by urea degradation.

The effects of cementation solution concentration on carbonate precipitation were assessed for 1, 0.5, and 0.25 M urea and $CaCl_2$ (Figure 7a,d,e). Overall, decreasing the solution concentration led to decreases in precipitate sizes (median volumes after 8 PV decreased from 4680 μm^3 at 1 M to 990 μm^3 at 0.5 M and 653 μm^3 at 0.25 M). The total number of individual calcium carbonate grains remained approximately constant, except at very low concentrations (0.25 M, Figure 7e) where nucleation was limited.

Lastly, the impact of injection processes on carbonate growth was explored (Figure 7a,f). Specifically, we altered the injection process by alternating between constant flow and no flow conditions such that the cementation solution was injected continuously for 5 h, followed by 5 h of quiescence (Figure 7f). During this time, only half of the cementation reagents (i.e., $CaCl_2$ and urea) were supplied to the bacteria compared with the base case. After 4 PV of cementation, the overall carbonate saturation was ∼0.16%, less than half of that in the base case. The increased residence time in proximity to oil interfaces also increases the inhibition of bacteria enzyme activity (recall from Figure 6) and hinders the overall $CaCO_3$ precipitation process. During this time, the consumption rate of calcite ions and urea is low (∼2−3%). One cause of the low consumption rate is the high Michaelis constant of urea (∼100 mM) for *S. pasteurii*,[44] which can be decreased significantly through strain screening or genetic engineering. Overall, the no-flow period during the injection did not provide any significant increase in calcium carbonate precipitation.

4. CONCLUSIONS

In this study, we present a novel MICP approach for enhanced oil recovery. In a microfluidic device with pore geometry and geochemistry representative of real geologic media, we showed the viability of injecting a bacteria-laden solution into preferential flow paths that biogenically induce carbonate precipitation to alter flow patterns within the subsurface. Specifically, reductions in the local porosity and pore connectivity of water-swept pathways (∼5% local reduction in porosity of water-swept regions) led to flow diversion away from the initially preferred pathways and into the oil-bearing regions. The flow diversion caused by MICP-EOR increased overall oil recovery by an additional ∼28% OOIP. To optimize the MICP-EOR, we performed a sensitivity analysis on bacterial growth and carbonate precipitation as well as the oil recovery as functions of cementation conditions (i.e., injection rate, concentration of cementation fluid, injection patterns) and revealed that the cementation process is limited by the rate of microbial urea decomposition.

AUTHOR INFORMATION

Corresponding Author

Wen Song − *Center for Subsurface Energy and the Environment, University of Texas at Austin, Austin, Texas 78712, United States;* orcid.org/0000-0003-1913-4503; Email: wensong@utexas.edu

Authors

Shunxiang Xia − *Center for Subsurface Energy and the Environment, University of Texas at Austin, Austin, Texas 78712, United States*

Artur Davletshin − *Center for Subsurface Energy and the Environment, University of Texas at Austin, Austin, Texas 78712, United States*

Complete contact information is available at: https://pubs.acs.org/10.1021/acs.energyfuels.3c02027

Author Contributions

S.X.: Conceptualization, methodology, investigation, writing—original draft, and visualization. A.D.: Image processing and methodology. W.S.: Funding acquisition, conceptualization, supervision, and writing—review and editing.

Notes

The authors declare no competing financial interest.

ACKNOWLEDGMENTS

The authors gratefully acknowledge funding from the United States Department of Energy (FE0031791). The authors thank Dr. Raluca Gearba-Dolocan from the Texas Materials Institute for discussions that improved the etching process of micromodels. In addition, the authors gratefully acknowledge Jonathan Ekman and Dr. Anil Shukla from Nikon Instruments for their assistance in setting up the microscopes.

REFERENCES

(1) OECD Publishing; OECD. *World Energy Outlook 2020*; Paris Organisation For Economic Co-Operation And Development OECD, 2020.

(2) Bartels, W.-B.; Mahani, H.; Berg, S.; Hassanizadeh, S. M. Literature Review of Low Salinity Waterflooding from a Length and Time Scale Perspective. *Fuel* **2019**, *236*, 338−353.

(3) Bahadori, A. *Fundamentals of Enhanced Oil and Gas Recovery from Conventional and Unconventional Reservoirs*; Gulf Professional Publishing, 2018.

(4) Moradi-Araghi, A.; Beardmore, D. H.; Stahl, G. A. The Application of Gels in Enhanced Oil Recovery: Theory, Polymers and Crosslinker Systems. *Water-Soluble Polym. Pet. Recovery* **1988**, 299−312.

(5) Zhai, K.; Yi, H.; Liu, Y.; Geng, Y.; Fan, S.; Zhu, D. Experimental Evaluation of the Shielded Temporary Plugging System Composed of Calcium Carbonate and Acid-Soluble Preformed Particle Gels (ASPPG) for Petroleum Drilling. *Energy Fuels* **2020**, *34* (11), 14023−14033.

(6) Jiang, N.-J.; Soga, K.; Kuo, M. Microbially Induced Carbonate Precipitation for Seepage-Induced Internal Erosion Control in Sand−

Clay Mixtures. *J. Geotech. Geoenviron. Eng.* **2017**, *143* (3), No. 04016100.
(7) Woodward, J. *An Introduction to Geotechnical Processes*; CRC Press: London, England, 2014. DOI: 10.1201/9781482265187.
(8) Shaffer, G. Long-Term Effectiveness and Consequences of Carbon Dioxide Sequestration. *Nat. Geosci.* **2010**, *3* (7), 464−467.
(9) DeJong, J. T.; Fritzges, M. B.; Nüsslein, K. Microbially Induced Cementation to Control Sand Response to Undrained Shear. *J. Geotech. Geoenviron. Eng.* **2006**, *132* (11), 1381−1392.
(10) Nassar, M. K.; Gurung, D.; Bastani, M.; Ginn, T. R.; Shafei, B.; Gomez, M. G.; Graddy, C. M. R.; Nelson, D. C.; DeJong, J. T. Large-scale Experiments in Microbially Induced Calcite Precipitation (MICP): Reactive Transport Model Development and Prediction. *Water Resour. Res.* **2018**, *54* (1), 480−500.
(11) Zhang, J.; Shi, X.; Chen, X.; Huo, X.; Yu, Z. Microbial-Induced Carbonate Precipitation: A Review on Influencing Factors and Applications. *Adv. Civ. Eng.* **2021**, *2021*, No. 9974027.
(12) Wu, J.; Wang, X.-B.; Wang, H.-F.; Zeng, R. J. Microbially Induced Calcium Carbonate Precipitation Driven by Ureolysis to Enhance Oil Recovery. *RSC Adv.* **2017**, *7* (59), 37382−37391.
(13) Song, C.; Elsworth, D. Microbially Induced Calcium Carbonate Plugging for Enhanced Oil Recovery. *Geofluids* **2020**, *2020*, No. 5921789.
(14) Cui, M.-J.; Zheng, J.-J.; Zhang, R.-J.; Lai, H.; Zhang, J. Influence of Cementation Level on the Strength Behaviour of Bio-Cemented Sand. *Acta Geotech.* **2017**, *12* (5), 971−986, DOI: 10.1007/s11440-017-0574-9.
(15) Minto, J. M.; Hingerl, F. F.; Benson, S. M.; Lunn, R. J. X-Ray CT and Multiphase Flow Characterization of a 'Bio-Grouted' Sandstone Core: The Effect of Dissolution on Seal Longevity. *Int. J. Greenhouse Gas Control* **2017**, *64*, 152−162.
(16) Wang, Y.; Soga, K.; DeJong, J. T.; Kabla, A. J. Effects of Bacterial Density on Growth Rate and Characteristics of Microbial-Induced CaCO3 Precipitates: Particle-Scale Experimental Study. *J. Geotech. Geoenviron. Eng.* **2021**, *147* (6), No. 04021036, DOI: 10.1061/(ASCE)GT.1943-5606.0002509.
(17) Achal, V.; Pan, X. Influence of Calcium Sources on Microbially Induced Calcium Carbonate Precipitation by Bacillus Sp. CR2. *Appl. Biochem. Biotechnol.* **2014**, *173* (1), 307−317.
(18) Sham, E.; Mantle, M. D.; Mitchell, J.; Tobler, D. J.; Phoenix, V. R.; Johns, M. L. Monitoring Bacterially Induced Calcite Precipitation in Porous Media Using Magnetic Resonance Imaging and Flow Measurements. *J. Contam. Hydrol.* **2013**, *152*, 35−43.
(19) Ma, L.; Pang, A.-P.; Luo, Y.; Lu, X.; Lin, F. Beneficial Factors for Biomineralization by Ureolytic Bacterium *Sporosarcina pasteurii*. *Microb. Cell Fact.* **2020**, *19* (1), 12.
(20) Larsen, J.; Poulsen, M.; Lundgaard, T.; Agerbæk, M. Plugging of Fractures in Chalk Reservoirs by Enzyme-Induced Calcium Carbonate Precipitation. *SPE Prod. Oper.* **2008**, *23* (4), 478−483.
(21) Wu, J.; Wang, X.; Wang, H.-F.; Zeng, R. J. Microbially Induced Calcium Carbonate Precipitation Driven by Ureolysis to Enhance Oil Recovery. *RSC Adv.* **2017**, *7* (59), 37382−37391.
(22) Lee, S. G.; Lee, H.; Gupta, A.; Chang, S.; Doyle, P. S. Site-selective in Situ Grown Calcium Carbonate Micromodels with Tunable Geometry, Porosity, and Wettability. *Adv. Funct. Mater.* **2016**, *26* (27), 4896−4905.
(23) Song, W.; Ogunbanwo, F.; Steinsbø, M.; Fernø, M. A.; Kovscek, A. R. Mechanisms of Multiphase Reactive Flow Using Biogenically Calcite-Functionalized Micromodels. *Lab Chip* **2018**, *18* (24), 3881−3891.
(24) Song, W.; de Haas, T. W.; Fadaei, H.; Sinton, D. Chip-off-the-Old-Rock: The Study of Reservoir-Relevant Geological Processes with Real-Rock Micromodels. *Lab Chip* **2014**, *14* (22), 4382−4390.
(25) Song, W.; Kovscek, A. R. Functionalization of Micromodels with Kaolinite for Investigation of Low Salinity Oil-Recovery Processes. *Lab Chip* **2015**, *15* (16), 3314−3325.
(26) Song, W.; Kovscek, A. R. Direct Visualization of Pore-Scale Fines Migration and Formation Damage during Low-Salinity Waterflooding. *J. Nat. Gas Sci. Eng.* **2016**, *34*, 1276−1283.
(27) Jian, G.; Fernandez, C. A.; Puerto, M.; Sarathi, R.; Bonneville, A.; Biswal, S. L. Advances and Challenges in CO2 Foam Technologies for Enhanced Oil Recovery in Carbonate Reservoirs. *J. Pet. Sci. Eng.* **2021**, *202*, No. 108447.
(28) Jian, G.; Alcorn, Z.; Zhang, L.; Puerto, M. C.; Soroush, S.; Graue, A.; Biswal, S. L.; Hirasaki, G. J. Evaluation of a Nonionic Surfactant Foam for CO2Mobility Control in a Heterogeneous Carbonate Reservoir. *SPE J.* **2020**, *25* (6), 3481−3493.
(29) Føyen, T.; Alcorn, Z. P.; Fernø, M. A.; Barrabino, A.; Holt, T. CO2Mobility Reduction Using Foam Stabilized by CO2- and Water-Soluble Surfactants. *J. Pet. Sci. Eng.* **2021**, *196*, No. 107651.
(30) Elmaloglou, A.; Terzis, D.; De Anna, P.; Laloui, L. Microfluidic Study in a Meter-Long Reactive Path Reveals How the Medium's Structural Heterogeneity Shapes MICP-Induced Biocementation. *Sci. Rep.* **2022**, *12* (1), No. 19553, DOI: 10.1038/s41598-022-24124-6.
(31) Wang, Y.; Soga, K.; DeJong, J. T.; Kabla, A. A Microfluidic Chip and Its Use in Characterising the Particle-Scale Behaviour of Microbial-Induced Calcium Carbonate Precipitation (MICP). *Geotechnique* **2019**, *69* (12), 1086−1094.
(32) Xiao, Y.; He, X.; Wu, W.; Stuedlein, A. W.; Evans, T. M.; Chu, J.; Liu, H.; Van Paassen, L. A.; Wu, H. Kinetic Biomineralization through Microfluidic Chip Tests. *Acta Geotech.* **2021**, *16* (10), 3229−3237.
(33) Jin, C.; Liu, H.; Guo, M.; Wang, Y.; Zhu, J. Experimental Study on Tailings Cementation by MICP Technique with Immersion Curing. *PLoS One* **2022**, *17* (8), e0272281 DOI: 10.1371/journal.-pone.0272281.
(34) *Publication: USDA ARS*. www.ars.usda.gov. https://www.ars.usda.gov/research/publications/publication/?seqNo115=188168 (accessed Apr 20, 2023).
(35) Arab, D.; Kantzas, A.; Bryant, S. L. Water Flooding of Oil Reservoirs: Effect of Oil Viscosity and Injection Velocity on the Interplay between Capillary and Viscous Forces. *J. Pet. Sci. Eng.* **2020**, *186*, No. 106691.
(36) Davletshin, A.; Ko, L. T.; Milliken, K.; Periwal, P.; Wang, C.-C.; Song, W. Detection of Framboidal Pyrite Size Distributions Using Convolutional Neural Networks. *Mar. Pet. Geol.* **2021**, *132*, No. 105159.
(37) Wani, K. M. N. S.; Mir, B. A. An Experimental Study on the Bio-Cementation and Bio-Clogging Effect of Bacteria in Improving Weak Dredged Soils. *Geotech. Geol. Eng.* **2021**, *39* (1), 317−334.
(38) Hassannayebi, N.; Jammernegg, B.; Schritter, J.; Arnold, P.; Enzmann, F.; Kersten, M.; Loibner, A. P.; Fernø, M.; Ott, H. Relationship between Microbial Growth and Hydraulic Properties at the Sub-Pore Scale. *Transp. Porous Media* **2021**, *139* (3), 579−593.
(39) Peng, J.; Liu, Z. Influence of Temperature on Microbially Induced Calcium Carbonate Precipitation for Soil Treatment. *PLoS One* **2019**, *14* (6), No. e0218396.
(40) Feyzi, H.; Chorom, M.; Bagheri, G. Urease Activity and Microbial Biomass of Carbon in Hydrocarbon Contaminated Soils. A Case Study of Cheshmeh-Khosh Oil Field, Iran. *Ecotoxicol. Environ. Saf.* **2020**, *199*, No. 110664.
(41) Hua, Z.; Lin, M.; Guo, J.; Xu, F.; Li, Z.; Li, M. Study on Plugging Performance of Cross-Linked Polymer Microspheres with Reservoir Pores. *J. Pet. Sci. Eng.* **2013**, *105*, 70−75.
(42) Song, C.; Chen, Y.; Wang, J. Plugging High-Permeability Zones of Oil Reservoirs by Microbially Mediated Calcium Carbonate Precipitation. *ACS Omega* **2020**, *5* (24), 14376−14383.
(43) Jeong, M. S.; Lee, J. H.; Lee, K. S. Critical Review on the Numerical Modeling of In-Situ Microbial Enhanced Oil Recovery Processes. *Biochem. Eng. J.* **2019**, *150*, No. 107294.
(44) Wu, Y.; Li, H.; Li, Y. Biomineralization Induced by Cells of *Sporosarcina pasteurii*: Mechanisms, Applications and Challenges. *Microorganisms* **2021**, *9* (11), 2396.